Electronic Research Archive

ERA, 31(4): 2019–2047.
DOI: 10.3934/era.2023104
Received: 18 December 2022
Revised: 21 January 2023
Accepted: 22 January 2023
Published: 16 February 2023

http://www.aimspress.com/journal/ERA

Research article

Novel lightweight connecting bracket design with multiple performance constraints based on optimization and verification process

Furong Xie[1], Yunkai Gao[1,*], Ting Pan[2], De Gao[2], Lei Wang[2], Yanan Xu[3] and Chi Wu[3]

[1] School of Automotive Studies, Tongji University, Shanghai 201804, China
[2] Process Research Center, Beiben Trucks Group Co., Ltd., Baotou 014000, China
[3] School of Aerospace, Mechanical and Mechatronic Engineering, The University of Sydney, Sydney, NSW 2006, Australia

* **Correspondence:** Email: gaoyunkai@tongji.edu.cn.

Abstract: In this paper, a complete optimization design verification process is proposed and a novel structure of connecting brackets is presented, solving the fatigue failure of chassis connecting brackets operating on harsh roads. First, an endurance road test and fatigue life analysis were applied to the truck equipped with the original brackets, verifying the fatigue damage of the structure. Based on the solid isotropic material with penalization method, a novel lightweight connecting bracket layout was obtained by using the method of moving asymptotes (MMA) for topology optimization under multiple working conditions with multiple performance constraints. Moreover, the derivatives of objective and constraint functions concerning design variables were applied for the MMA. Considering manufacturability and functionality, the improved model based on the topology optimization results was further optimized by size optimization. Finally, fatigue life analysis and an endurance road test were conducted using the optimal design. Compared with the original structure, the novel brackets showed better stiffness, strength and fatigue performance while reducing the total mass by 15.2%. The whole optimization and validation process can provide practical ideas and value for developing multi-performance suspensions in the pre-product development stage.

Keywords: lightweight design; connecting bracket; topology optimization; size optimization; fatigue failure

1. Introduction

As a crucial method to improve the efficiency of freight transport, globally, heavy-duty transportation has become the main development direction for freight transport [1]. With the burgeoning prosperity of the long-distance freight and urban logistics industry, the demand for cargo trucks is gradually increasing. As shown in Figure 1, the connecting brackets in blue are an essential connecting part of the chassis in the cargo truck, bearing the load transmitted by the road excitation. However, the occurrence of harsh road conditions in heavy-duty transportation is inevitable. Therefore, to mitigate the impact on the vehicle and ensure safety, obtaining a lightweight structure with high performance via a complete design optimization and verification process is the key to the performance development stage of the vehicle suspension.

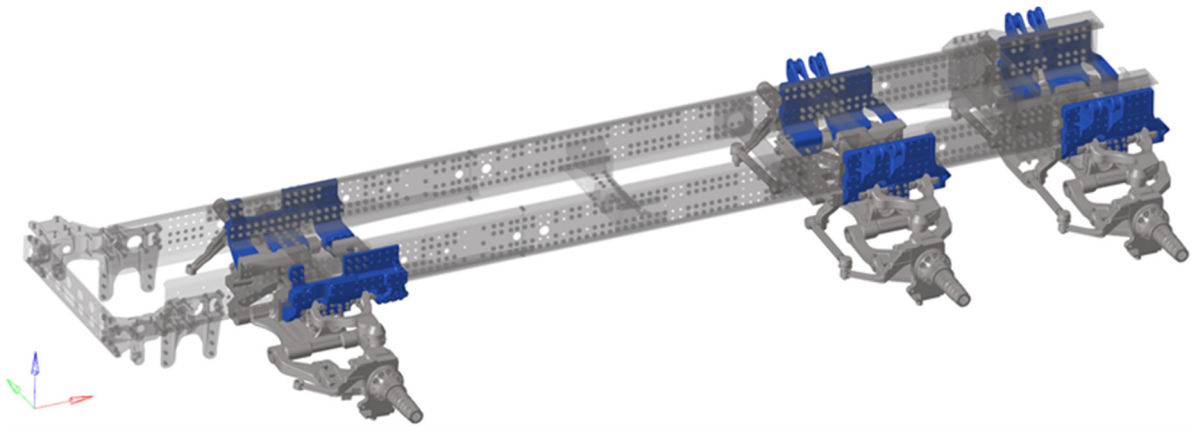

Figure 1. Model of connecting bracket.

Topology optimization does not involve specific structural dimensions, but it can suggest the best conceptual design solution [2]. However, it needs to be modified appropriately according to engineering rationality as a conceptual design result. The improved design solution is then optimized by size to obtain the optimal structure. The research of topology optimization in continuum structure can be traced back to 1981 [3], i.e., when the microstructure concept was first introduced into the optimization problem by minimizing the compliance of the solid plate. Cheng and Olhoff employed the plate thickness function as the design variable and took both maximum and minimum allowable thickness values into account. Bendsoe and Kikuchi [4] proposed a homogenization method for structural topology optimization, describing the structural topology in terms of microstructural concepts and homogenization methods. The variable-density method transforms the topology optimization problem into an optimal distribution of materials problem, inspired by the homogenization method. Bendsoe and Sigmund [5] conducted an in-depth study of material interpolation models for variable-density methods by theoretically investigating various material interpolation models for different variable-density methods. Martínez [6] discussed the theoretical convergence of the solid isotropic material with penalization (SIMP) method for topology optimization. Stolpe and Svanberg [7] presented the ramp approximation of material properties method to find the optimal distribution of two linearly elastic materials such that the compliance was minimized. To minimize the compliance, Zhang and Ren [8] proposed an optimality criteria method

for the topology optimization of continuum structures based on SIMP. The examples showed that the algorithm had good convergence and application values. Zuo et al. [9] presented a new sensitivity reanalysis of static displacement for arbitrary changes of design variables; it has great potential application in the gradient-based structural optimization. Zuo et al. [10] developed a modified topology optimization method by adding manufacturing and machining constraints to the topology optimization formulation while applying the MMA and wavelets to solve this optimization problem. Gao et al. [11] developed an adaptive continuation method for the buckling-constrained topology optimization of continuum structures by using a SIMP model. Besides a mass constraint, a cost constraint was also considered in the compliance minimization problems. Xu et al. [12] proposed a novel solution to the stress-constrained multi-material topology optimization problem based on the ordered SIMP method; an adjoint sensitivity analysis was performed and the optimization problem was solved by using an MMA optimizer. The variable-density method has also been widely used for optimization problems in various fields [13−15].

In the past few decades, topology and size optimizations methods have been widely used to redesign and achieve better performance of vehicle components, such as stiffness, strength, vibration, and fatigue. Liu et al. [16] explored the topology optimization and sizing optimization in the lightweight design of frames for energy-saving vehicles, aiming to mitigate the stress concentration and excessive local deformation while reducing the frame's weight by more than 15.0%. Torstenfelt and Klarbring [17] developed a structural optimization method for a single product which was extended for the optimization of a family of products to allow size, shape, and topology optimization to be accomplished simultaneously. Wang et al. [18] applied topology optimization in the optimization design of the traction battery enclosure; they combined both the weighted compliance and the mean frequency to a single objective while constraining the volume to lightweight during the optimization process. Cho et al. [19] applied CFRP-AL honeycomb sandwich composites to the under-frame and roof structures; the size optimization method was subsequently applied to derive a lightweight composite hybrid carbody design. Lu et al. [20] proposed a comprehensive solution for bus frame design to bridge multi-material topology optimization and cross-sectional size optimization; they used SIMP to transform the multi-material selection problem into a pure topology optimization problem. Bai et al. [21] proposed a novel bridging method and applied it to a real automobile body example to transform the topological results into a lightweight, thin-walled frame structure that satisfies the stiffness and manufacturing requirements. Ma et al. [22] solved a lightweight design problem by utilizing the methods of topology and thickness optimization to redesign a new turnover frame. Sun et al. [23] proposed a multi-objective multi-material topology optimization method to determine the layout of welding lines for tailor-welded blank structures. The static stiffness and dynamic frequency criteria were addressed for multiple load cases by using compromise programming and mean frequency. Zhang et al. [24] applied topology optimization and size optimization to the front-end structures of the body-in-white to simultaneously improve the static stiffness and crashworthiness. Munk and Miller [25] mentioned that constraining the strength of components through topology optimization could substantially improve component load capacity and fatigue life.

In this paper, a complete optimization and verification process is proposed; it offers practical ideas and value in the early stage of product development. In the optimization stage of the process, topology and size optimization are used to obtain new connecting brackets with multiple performance constraints. In Section 2, the vehicle endurance road test and fatigue analysis that were applied to the

original bracket are discussed; we show that the bracket was damaged more severely during off-roading, so loading boundary conditions were extracted based on the dynamic load spectrum for the subsequent optimization. The SIMP method is demonstrated, and the design sensitivity is calculated in Section 3, while the size optimization is presented based on the topology optimization results. The optimal structure is validated in Section 4, and conclusions are drawn in Section 5. The flowchart is shown in Figure 2.

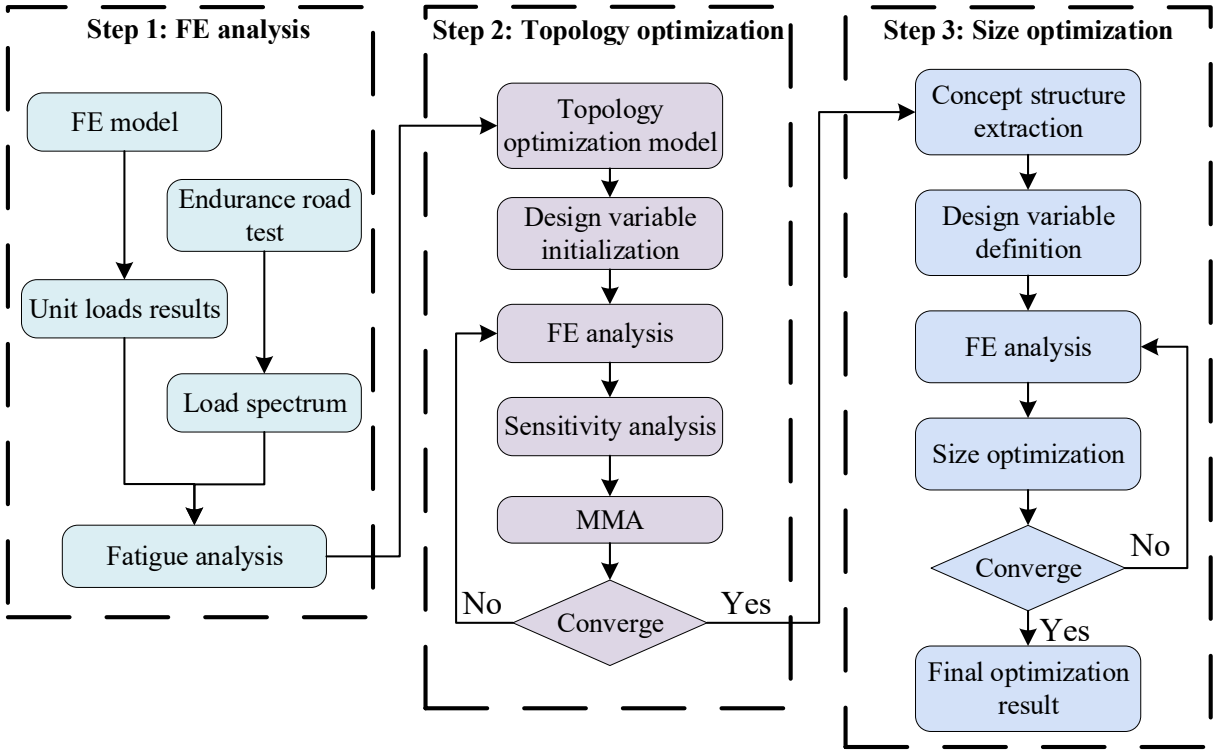

Figure 2. Flowchart of optimization design.

2. Finite element model of the connecting bracket

2.1. Finite element model

The symmetrical structures named connecting brackets are the major connecting parts of the chassis of the three-axle cargo truck; they are fixed to the frame by multiple bolts and secure the gearbox housing. The original finite element model was discretized with tetrahedral elements and the element size was set to 10 mm, the material parameters of which are shown in Table 1. As shown in Figure 3, the triangles illustrate that the nodes have zero degrees of freedom. The loading positions are the suspension hardpoints with the number on the connecting bracket. In the figure, the suspension system application locations include coil spring loading points 1 and 6, Y-shaped upper and lower control arm loading points 2–5 and 7–10 and loading points of the wheel side tie rods 11 and 12.

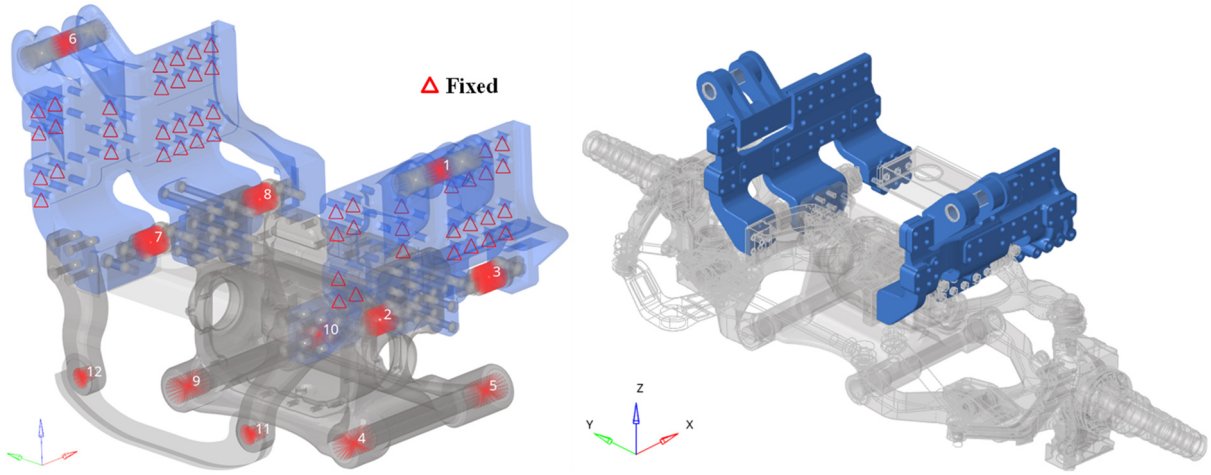

(a) Bracket with gearbox housing (b) Bracket with control arm

Figure 3. Original finite element model.

Table 1. Material properties.

Symbol	Parameter for metal material	Value
E_m	Young's modulus	216,000 MPa
σ_s	Yield strength	1189 MPa
σ_b	Tensile strength	1308 MPa
ν_{m12}	Poisson's ratio	0.3
ρ_m	Density	7900 kg/m^3

2.2. Endurance test and fatigue analysis procedure

The connecting brackets are the main chassis connection components; their stiffness, strength and fatigue life have a significant impact on the safety of the whole vehicle. Therefore, a vehicle endurance road test was applied to a three-axle truck with the original connecting bracket. Furthermore, the fatigue life of the original connecting bracket finite element model was predicted, and the accuracy of the fatigue life analysis results was verified through the experimental results of bracket damage locations.

The fatigue life is commonly calculated by considering the alternating and mean stresses, which can be generated by the superposition of the unit static load stress field and load spectrum in quasi-static fatigue analysis. The effective loading cycles are extracted by utilizing a suitable cycle counting method, such as the uniaxial rainflow cycle counting method and the multiaxial cycle counting method respectively proposed by Lee et al. [26] and Wang and Brown [27]. Two fatigue analysis methods are commonly applied in variable amplitude multiaxial loading. One is the equivalent stress or strain method, and the other is the critical plane method. The fatigue damage parameters are defined based on the cumulative equivalent stress or strain values from a multiaxial rainflow reversal counting method in the equivalent stress or strain method [26]. Jeong et al. [28] employed an equivalent stress method based on the multiaxial cycle counting method and Basquin relation to consider the transient stress history in a multiaxial stress state. In this paper, the stress response of the original structure at

the loading points under unit loads of six degrees of freedom (unit forces and unit moments in three directions X, Y and Z) was analyzed by using the finite element method. The stress response spectra at hardpoint positions were acquired by combining the loading spectra acquired from the endurance road test and unit loads results. The load spectra are the curves of forces and moments versus time in the X, Y and Z directions. The relationship between cyclic stress amplitude and average stress was corrected by applying the Goodman curve via the multiaxial cycle counting method. Furthermore, the cumulative damage value D was obtained by adopting the fatigue damage accumulation theory based on Miner's rule [28] under the off-road load spectrum. After applying the off-road load spectrum, the fatigue damage cloud under the effect of a cycle load spectrum was constructed as presented in Figure 4. In the figure, the fatigue damage becomes significantly extreme in the corner positions. The fatigue cumulative damage value D converted to target distance is as follows:

$$D = D_0 \frac{s_t}{s_0} = \frac{1}{N} \frac{s_t}{s_0} \tag{1}$$

where D_0 is the maximum value of fatigue damage under a single cycle in Figure 4 and s_0 represents the mileage corresponding to a cycle load spectrum, which was 3.7 km in this study; s_t is the target mileage, and it was set to be 6000 km; N represents the fatigue life corresponding to a single-cycle load level.

The cumulative damage value D of brackets reached 1.938, 2.822 and 7.049×10^{-3}, respectively, indicating a high probability of fatigue damage to the bracket. The cumulative damage D should be lower than 1. During the road test for the original connecting bracket, the results showed significant cracks below the bolt holes of the bracket-frame connection, as shown in Figure 4(a). Furthermore, the part below the connecting bolt hole of the bracket and the frame had been broken, as shown in Figure 4(b). Thus, the test results of finite element analysis verified the fatigue damage.

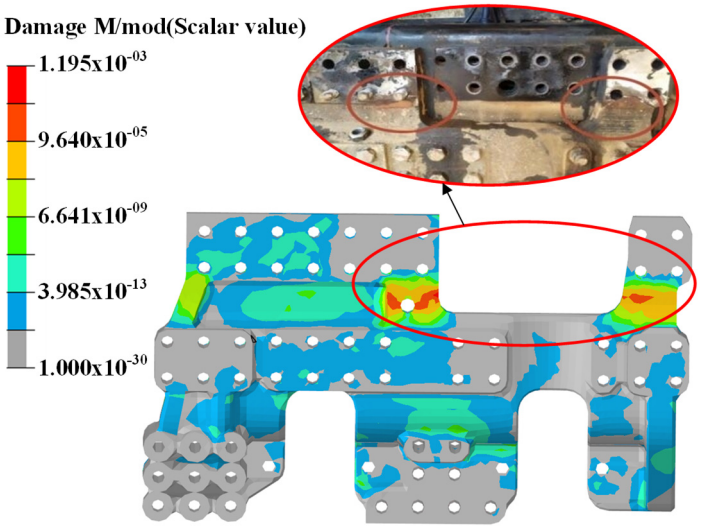

(a) Bracket in 1st axle

Continued on next page

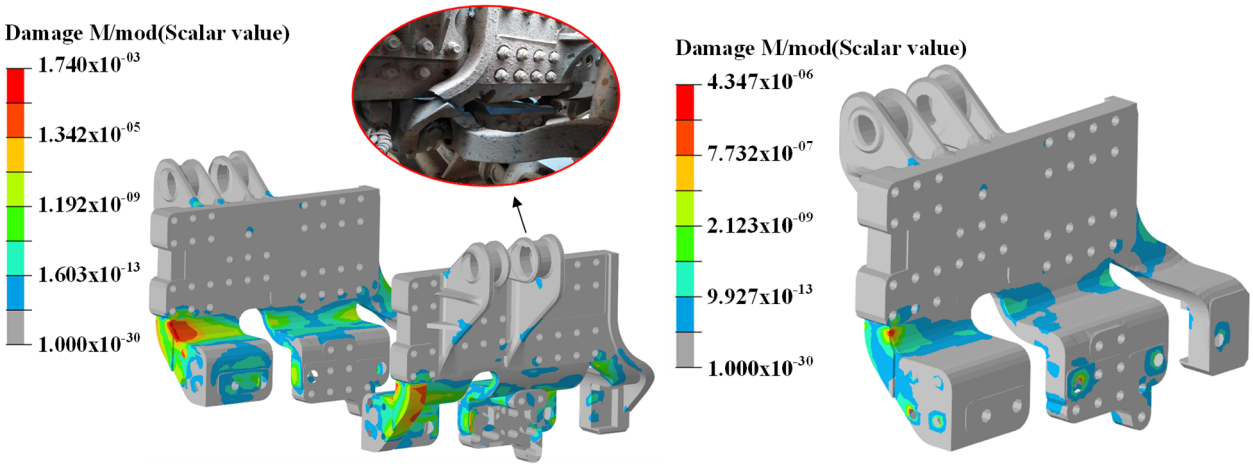

(b) Bracket in 1st axle (c) Bracket in 3rd axle

Figure 4. Fatigue damage under the effect of a single-cycle load spectrum.

The endurance road test results and fatigue life analysis showed that the original design of the connecting bracket structure did not meet the engineering requirements, and that the bracket fatigue was damaged. Therefore, it is necessary to design novel connecting brackets with higher strength, higher stiffness and a lighter weight to guarantee structural performance under harsh driving road conditions. The optimization process should first define the topological space that envelops the bracket structure. The new topology model is thus given in Figure 5; it has a larger design area below, and the lower end of the bracket is connected to the lower Y-shaped control arm. Also, the new structure increases the design space at the bottom of the gearbox housing to form an integral bridge box connecting bracket.

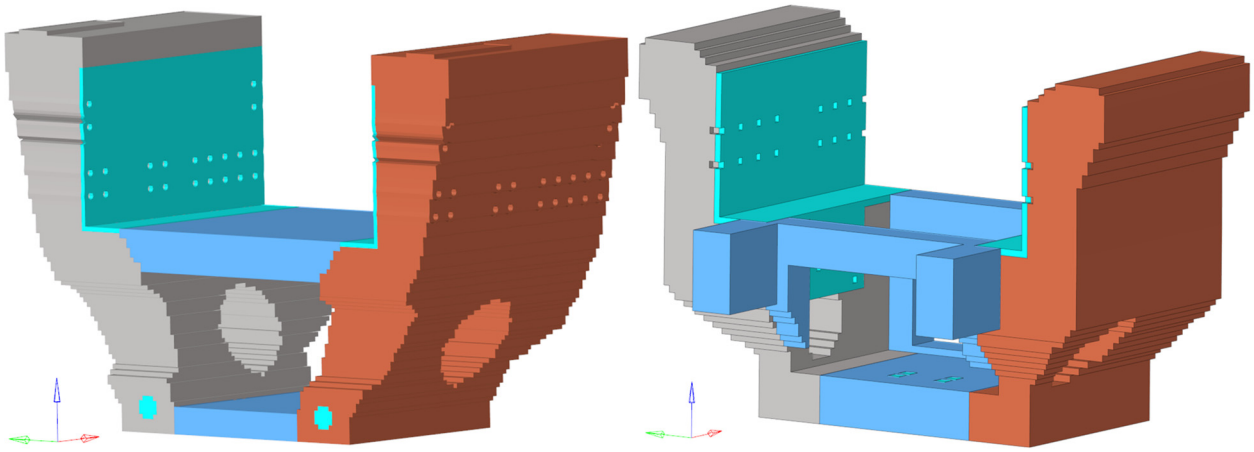

(a) First axle (b) Second axle

Continued on next page

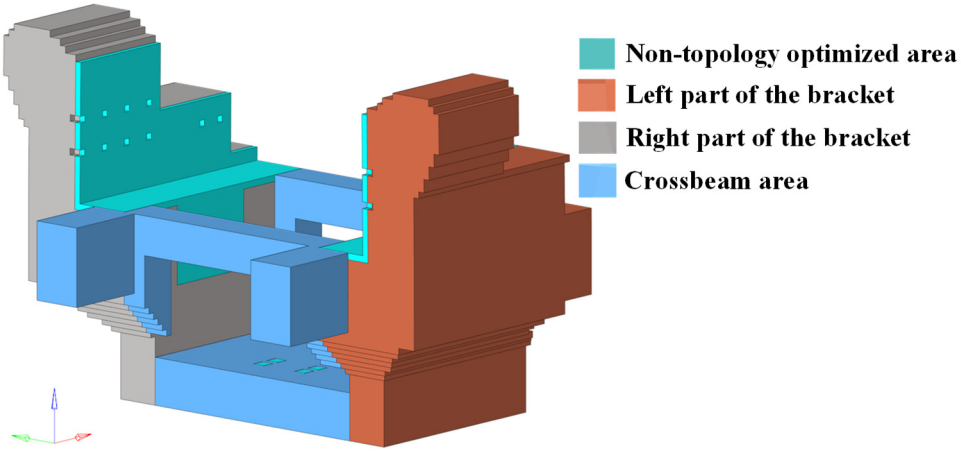

(c) Third axle

Figure 5. Topology model of the connecting bracket.

2.3. Loading boundary conditions

Haftka et al. [29] mentioned that equivalent static loads were calculated by multiplying some dynamic factors by dynamic loads in engineering applications. The structure was optimized based on these loading conditions. The direction of the equivalent static load is generally the same as the direction of the dynamic load, and the dynamic factors should be determined according to the dynamic effects, such as the peak of the curve in the time domain and the duration of the peak. The dynamic loads in this study were obtained from the vehicle endurance road test, independent of the design variables. The converted load sets were applied as external loads according to the engineering experience, and this changed a dynamic loading into the multiple static loading conditions shown in Table 2, while also considering the actual situation to add the torsion condition. Under each working condition, force and moment in the non-coordinate axis direction were applied at each loading point, with load magnitudes ranging from 10^3−10^7.

This study considers that the vehicle is affected by loads of the above five working conditions under off-road conditions. The maximum acceleration of the vehicle under different working conditions was determined by analyzing the road spectra derived from the road test and engineering experience. Then, by multiplying by the safety factor, the limit loads under different working conditions were finally obtained for analysis and optimization. For example, in the case of the bumping working condition in Table 2, the vertical acceleration value of 3.5 g was first determined and multiplied by a safety factor of 1; then, we obtained an FZ of $3.5Z_0$. Z_0 is the support force of the ground on the wheel under static and stable conditions. FX, FY and FZ are the forces in X, Y, and Z directions under the vehicle coordinate system. From the safety perspective, the effect of the equivalent static loads on the bracket must be equal to or greater than the effect of the dynamic load on the bracket at any critical moment. The static loads were applied to the original bracket finite element model for stress analysis to validate this boundary condition. The analysis results are shown in Figure 6. The stress concentration damage location is consistent with the fatigue cumulative damage analysis and test results.

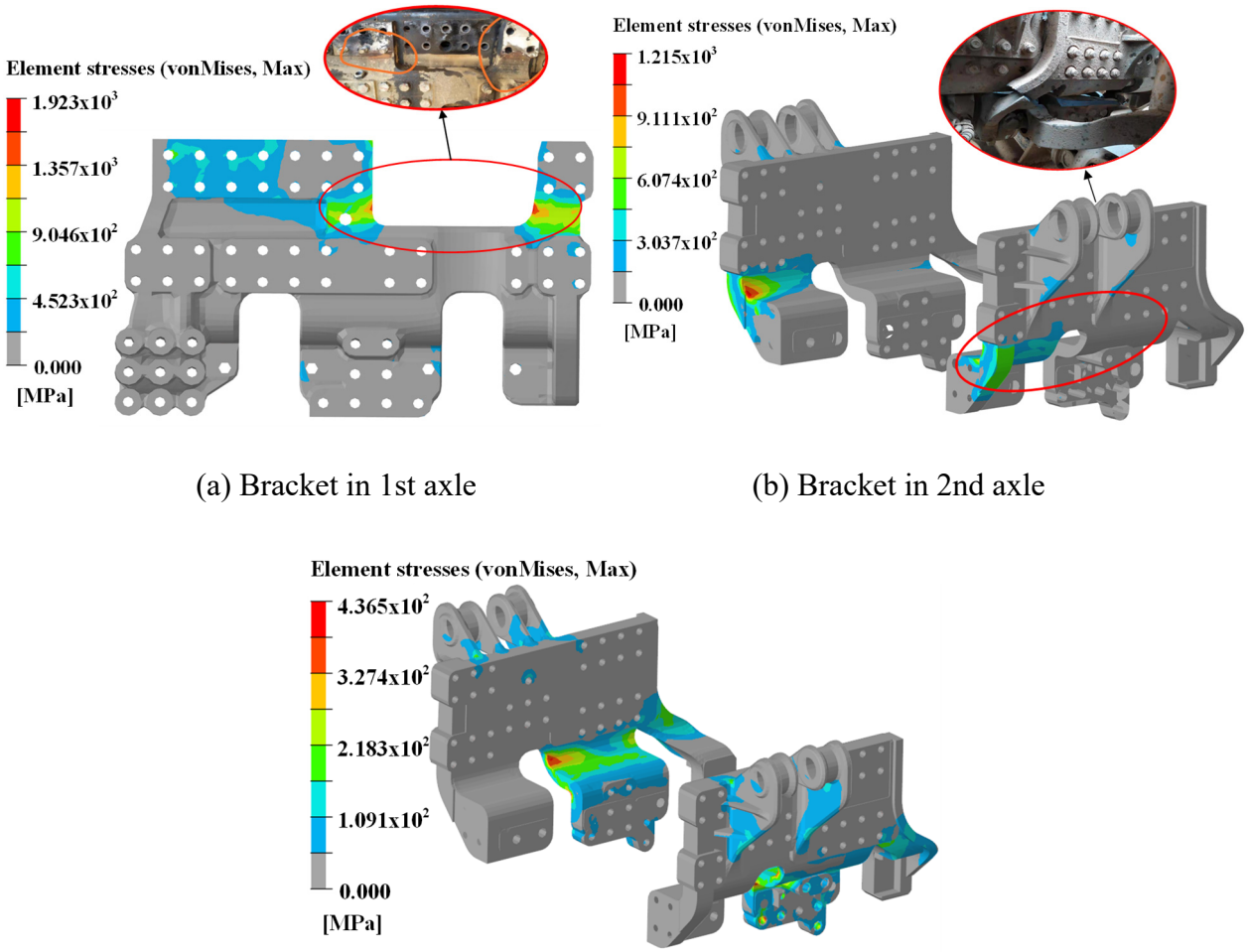

(a) Bracket in 1st axle

(b) Bracket in 2nd axle

(c) Bracket in 3rd axle

Figure 6. Stress amplitude distribution.

Table 2. Vehicle limit working conditions.

Working condition	FX	FY	FZ	Description
Bumping	0	0	$3.5Z_0$	Vertical acceleration: 3.5 g, safety factor: 1
Driving	$0.7 \times 2.5Z_0$	0	$2.5Z_0$	Vertical impact acceleration: 2.5 g, longitudinal acceleration: 0.7 g
Acceleration steering	$0.4 \times 2.0Z_0$	$0.3 \times 2.0Z_0$	$(1 + 2.0 \times 0.3) \times Z_0$	lateral acceleration: 0.3 g, driving resistance: 0.4 g, vertical impact acceleration: 1 g, safety factor: 2
Compound	1 g	0.4×2.5 g	2.5 g	-
Torsion	-	-	-	The front suspension is applied; 6° of torsion angle to test the cockpit

To optimize the structure to achieve better performance, the connecting bracket should meet the following requirements.

1) To ensure the safety and durability of the product, the fatigue life analysis of novel connecting brackets should be conducted and verified by a vehicle endurance road test.

2) The connecting bracket should have high overall stiffness, and the deformation of loading points under optimized conditions should not be greater than the empirical displacement value of the original casting under harsh extreme loading conditions. According to the different working conditions, the maximum deformation at loading points does not exceed a 0.9−3 mm range.

3) Considering the dynamic performance of the structure and, according to the peak response curve of the endurance road test, the first-order constraint mode of the optimized connecting bracket should not be less than 150 Hz.

4) The connecting bracket should maintain enough strength to avoid fatigue failure. A simple empirical formula should be used to calculate the fatigue strength: $\sigma_1 = 0.27(\sigma_s + \sigma_b)$, where σ_1 is the fatigue strength, σ_s is the yield strength, and σ_b is the maximum tensile strength [30]. The support was made of special steel, as listed in Table 1. Therefore, the value of σ_1 was 650 MPa in this study.

3. Optimization

3.1. Topology optimization

3.1.1. Methodology

The material interpolation model plays a significant role in topology optimization, which is the basis for most subsequent optimization methods. The SIMP method is based on isotropic materials and artificially assumes some correspondence between the density of the element and the physical properties of the material [31]. The relative density of each element is used as the design variable x. Each element has a unique design variable in the interval [0, 1], which makes the procedure simple to implement and computationally efficient. Based on the definition of the SIMP method, the constitutive material matrix of element i can be expressed as follows:

$$\begin{cases} \rho_i = x_i \rho_0 \\ \mathbf{E}_i = \mathbf{E}_0 + x_i^p (\mathbf{E} - \mathbf{E}_0) \end{cases} \tag{2}$$

where x_i is the relative density of element i and ρ_0 is the actual structural material; ρ_i denotes the corresponding material density of relative density. $\mathbf{E}_0$ is the constitutive matrix of the artificial material that is required to avoid singularity; $\mathbf{E}$ represents the constitutive matrix of the real physical quantity of the material. Here, x_i is regarded as a topological variable and p is the penalization parameter, which serves to penalize the intermediate density values when the values of the design variables are between (0, 1) so that the intermediate density values gradually converge to the 0/1 ends, enabling the topological optimization model of continuous variables to approximate the original {0, 1} discrete variable optimization model.

According to the principle of minimum potential energy, the stiffness matrix can be calculated as follows:

$$\mathbf{K} = \sum_{i=1}^{n} \int \mathbf{B}_i^T \mathbf{E}_i \mathbf{B}_i dv_i \tag{3}$$

where **K** is the global stiffness matrix and $\mathbf{B}_i$ is the strain-displacement matrix of element *i*, as defined by derivatives of the element shape functions; v_i is the volume of element *i*.
Similarly, the mass matrix can be obtained as follows:

$$\mathbf{M} = \sum_{i=1}^{n} \int \rho_i \mathbf{N}^T \mathbf{N} dv_i \tag{4}$$

where **N** is the element shape function matrix.

However, numerical instabilities tend to occur in the topology optimization of continuum structures, resulting in common problems such as mesh-dependence and checkerboard patterns in classical density-based topology optimization [32]. To obtain an optimal structure with clear boundaries, the topological sensitivity is filtered with a density-based filtering technique. For the optimization objective and the constrained sensitivity, the new topological sensitivity can be calculated as follows:

$$\frac{\partial \hat{f}}{\partial x_k} = (x_k)^{-1} \frac{1}{\sum_{i=1}^{n} \omega_i} \sum_{i=1}^{n} \omega_i x_i \frac{\partial f}{\partial x_i} \tag{5}$$

where $\partial f / \partial x_i$ is the topological sensitivity of the response function *f* with respect to the design variable x_i in element *i*; ω_i is a weighted function, which can be calculated as

$$\omega_i = r_{min} - dist(i,k) \tag{6}$$

where r_{min} is the filter radius and $dist(i,k)$ denotes the distance between the central coordinates of element *i* and element *k*.

3.1.2. Mathematical formulation of optimization

In the definition of the optimization problem, the objective is to minimize the structural volume while constraining structural strength, stiffness and low-order frequency under the five working conditions in order to meet the lightweight requirement. The initial values for all of the topological variables were set to 0.5. Accordingly, the design problem can be formulated as follows:

$$\begin{cases} \text{find: } \mathbf{x} = [x_1, x_2, x_3, \dots, x_n]^T \\ \text{Minimize: Volume Fraction}(x) = \frac{\sum_{i=1}^{n} x_i v_i}{V_0} \\ Subject\ to: \mathbf{K}\mathbf{U}_l = \mathbf{F}_l, l = 1,2,3 \dots 5 \\ \qquad (\mathbf{K} - \omega_k^2 \mathbf{M})\boldsymbol{\varphi}_k = \mathbf{0} \\ \qquad \sigma_{vm,i}^{l} \le \tilde{\sigma}_0, i = 1,2,3, \dots n; l = 1,2,3 \dots 5 \\ \qquad d_j^l \le \left|\tilde{d}^l\right|, j = 1,2,3, \dots 12 \\ \qquad \omega_k \ge \widetilde{\omega}_0 \\ \qquad x_i \in [0,1] \end{cases} \tag{7}$$

where V_0 is the total volume of the topology space, $\sigma_{vm,i}^{l}$ is the von Mises stress of the element *i* under the l^{th} working condition, d_j^l is the displacement amplitude of the j^{th} loading point under the l^{th} working condition and ω_k is the k^{th} constrained mode of the structure.

The MMA [33] is employed here to find the optimal solution to the defined optimization problem.

The convergence criterion of the MMA is that the maximum difference of the design variables in the last two consecutive iterations is less than the given tolerance, denoted as follows:

$$\|x_\delta - x_{\delta-1}\|_\infty \le \varsigma \tag{8}$$

where x_δ denotes the vector of design variables at the δ^{th} iteration and ς (= 0.005 here) is the prescribed convergence tolerance.

3.1.3. Sensitivity analysis

Sensitivity analysis is an essential part of the gradient-based topological optimization method since it is required to provide gradient information to the mathematical programming algorithm to solve the optimal solution.

For modal sensitivity [34], ω_k denotes the eigenvalue of the k^{th}-order constrained mode of the structure, and the equation of motion is as follows:

$$(\mathbf{K} - \omega_k^2 \mathbf{M})\boldsymbol{\varphi}_k = \mathbf{0} \tag{9}$$

where $\mathbf{M}$ represents the overall mass matrix and $\boldsymbol{\varphi}_\mathbf{k}$ is the corresponding vibrational mode of the k^{th}-order mode. Equation (9) is differentiated with respect to the design variables x_i, as follows:

$$(\mathbf{K} - \omega_k^2 \mathbf{M})\frac{\partial \boldsymbol{\varphi}_k}{\partial x_i} + \left(\frac{\partial \mathbf{K}}{\partial x_i} - \omega_k^2 \frac{\partial \mathbf{M}}{\partial x_i}\right)\boldsymbol{\varphi}_k - \frac{\partial \omega_k^2}{\partial x_i}\mathbf{M}\boldsymbol{\varphi}_k = \mathbf{0} \tag{10}$$

Multiply $\boldsymbol{\varphi}_k^T$ and orthogonalize $\mathbf{M}$ on the left side to obtain the modal sensitivity:

$$\frac{\partial \omega_k}{\partial x_i} = \frac{1}{2\omega_k}\boldsymbol{\varphi}_k^T\left(\frac{\partial \mathbf{K}}{\partial x_i} - \omega_k^2 \frac{\partial \mathbf{M}}{\partial x_i}\right)\boldsymbol{\varphi}_k \tag{11}$$

For displacement sensitivity [35,36], full differentiation of the equation $\mathbf{KU} = \mathbf{F}$ is required:

$$\begin{cases} \dfrac{\partial \mathbf{K}}{\partial x_i}\mathbf{U} + \mathbf{K}\dfrac{\partial \mathbf{U}}{\partial x_i} - \dfrac{\partial \mathbf{F}}{\partial x_i} = \mathbf{0} \\ \dfrac{\partial \mathbf{U}}{\partial x_i} = -\mathbf{K}^{-1}\dfrac{\partial \mathbf{K}}{\partial x_i}\mathbf{U} \end{cases} \tag{12}$$

A virtual unit load is introduced here, and only the component corresponding to the j^{th} node in this load vector is 1, while the rest of the components are 0. The following deduction can be performed:

$$\begin{cases} U_j = \mathbf{F}_j^T\mathbf{U} \\ \dfrac{\partial U_j}{\partial x_i} = \mathbf{F}_j^T\dfrac{\partial \mathbf{U}}{\partial x_i} = -\mathbf{U}_{ij}^T\dfrac{\partial \mathbf{K}}{\partial x_i}\mathbf{U},\ while\ \mathbf{KU}_{ij} = \mathbf{F}_j \end{cases} \tag{13}$$

For the displacement $\mathbf{u}_j = (u_1, u_2, u_3)$ in the non-coordinate axis direction, u_1, u_2 and u_3 are the components of the displacement $\mathbf{u}_j$ on the X, Y and Z axes, respectively. The sensitivity of the displacement amplitude $|\mathbf{u}_j| = \sqrt{u_1^2 + u_2^2 + u_3^2}$ is derived as follows:

$$\begin{aligned}\frac{\partial|\mathrm{u}_j|}{\partial x_i}&=\frac{1}{\sqrt{u_1^2+u_2^2+u_3^2}}\left(u_1\frac{\partial u_1}{\partial x_i}+u_2\frac{\partial u_2}{\partial x_i}+u_3\frac{\partial u_3}{\partial x_i}\right)\\&=-\frac{1}{\sqrt{u_1^2+u_2^2+u_3^2}}(u_1\mathrm{U}_{i1}^T+u_2\mathrm{U}_{i2}^T+u_3\mathrm{U}_{i3}^T)\frac{\partial \mathrm{K}}{\partial x_i}\mathrm{U}\\&=-\frac{1}{\sqrt{u_1^2+u_2^2+u_3^2}}u_j\mathrm{U}_{ij}^T\frac{\partial \mathrm{K}}{\partial x_i}\mathrm{U}\end{aligned} \tag{14}$$

For the stress sensitivity [37−39], the following interpolation scheme can be performed for the elemental stress to avoid the singular solution problem that occurs during stress optimization:

$$\boldsymbol{\sigma}_i = x_i^q \mathbf{E}_0 \mathbf{B}_i \mathbf{u}_i \tag{15}$$

where $\mathbf{B}_i$ is the strain-displacement matrix of element i at the integral point and q is the *s*tress interpolation penalty parameter; q is equal to 0.5 here.

To evaluate the global maximum stress, the P-Norm function is used here to describe the stress of the structure, thus circumventing the constraints on the stress of each element. The global maximum von Mises stress can be written as follows:

$$\begin{cases}\bar{\sigma}_{PN} = \left(\sum_{i=1}^n \bar{\sigma}_i^{p_n}\right)^{\frac{1}{p_n}}\\ while:\\ \bar{\sigma}_i = \frac{1}{\sqrt{2}}\sqrt{\left(\sigma_x-\sigma_y\right)^2+\left(\sigma_y-\sigma_z\right)^2+(\sigma_z-\sigma_x)^2+6\left(\tau_{xy}^2+\tau_{yz}^2+\tau_{zx}^2\right)}\\ \qquad = (\boldsymbol{\sigma}_i^T\mathbf{T}\boldsymbol{\sigma}_i)^{\frac{1}{2}}\\ \boldsymbol{\sigma}_i = \left(\sigma_x,\sigma_y,\sigma_z,\tau_{xy},\tau_{yz},\tau_{zx}\right)^T\\ \mathbf{T} = \begin{bmatrix}1 & -0.5 & -0.5 & & & \\ -0.5 & 1 & -0.5 & & & \\ -0.5 & -0.5 & 1 & & & \\ & & & 3 & & \\ & & & & 3 & \\ & & & & & 3\end{bmatrix}\end{cases} \tag{16}$$

where $\boldsymbol{\sigma}_i$ is the stress vector of element i and $\mathbf{T}$ is the coefficient matrix.

The global maximum stress $\bar{\sigma}_{PN}$ and the derivative of the von Mises stress of element i with respect to the k^{th} design variable can be obtained from the adjoint method as follows:

$$\begin{cases}\frac{\partial \bar{\sigma}_{PN}}{\partial x_k} = \bar{\sigma}_{PN}^{1-p_n}\left(\sum_{i=1}^n \bar{\sigma}_i^{p_n-1}\frac{\partial \bar{\sigma}_i}{\partial x_k}\right), k = 1,2,\dots n\\ \frac{\partial \bar{\sigma}_i}{\partial x_k} = \frac{\partial \bar{\sigma}_i}{\partial \boldsymbol{\sigma}_i}\frac{\partial \boldsymbol{\sigma}_i}{\partial x_k}\\ \frac{\partial \bar{\sigma}_i}{\partial \boldsymbol{\sigma}_i} = \frac{1}{2}(\boldsymbol{\sigma}_i^T\mathbf{T}\boldsymbol{\sigma}_i)^{-\frac{1}{2}}2\boldsymbol{\sigma}_i^T\mathbf{T} = \bar{\sigma}_i^{-1}\boldsymbol{\sigma}_i^T\mathbf{T}\end{cases} \tag{17}$$

Equation (15) is brought into the above equation for calculation. As both the constitutive matrix and strain matrix of the real element are independent of the design variables, the partial derivative of the elemental stress vectors concerning the design variable can be obtained as follows:

$$\begin{aligned}\frac{\partial \boldsymbol{\sigma}_i}{\partial x_k}&=qx_i^{q-1}\mathbf{E}_0\mathbf{B}_i\mathbf{u}_i\frac{\partial x_i}{\partial x_k}+x_i^q\mathbf{E}_0\mathbf{B}_i\frac{\partial \mathbf{u}_i}{\partial x_k}\\&=qx_i^{q-1}\mathbf{E}_0\mathbf{B}_i\mathbf{u}_i\frac{\partial x_i}{\partial x_k}+x_i^q\mathbf{E}_0\mathbf{B}_i\mathbf{L}_i\frac{\partial \mathbf{u}}{\partial x_k}\\&=qx_i^{q-1}\mathbf{E}_0\mathbf{B}_i\mathbf{u}_i\frac{\partial x_i}{\partial x_k}-x_i^q\mathbf{E}_0\mathbf{B}_i\mathbf{L}_i\mathbf{K}^{-1}\frac{\partial \mathbf{K}}{\partial x_k}\mathbf{u}\end{aligned} \tag{18}$$

For the first term on the right-hand side of the above equation, the term is 0 when $i \neq k$. For the second term on the right-hand side, the nodal displacement of element i is integrated into the global displacement by introducing $\mathbf{u}_i = \mathbf{L}_i\mathbf{u}$. The stress sensitivity is collapsed to obtain the following:

$$\begin{aligned}\frac{\partial \bar{\sigma}_{PN}}{\partial x_k}=&\bar{\sigma}_{PN}^{1-p_n}\left(\sum_{i=1}^n \bar{\sigma}_i^{p_n-2}qx_i^{q-1}\boldsymbol{\sigma}_i^T\mathbf{T}\mathbf{E}_0\mathbf{B}_i\mathbf{u}_i\frac{\partial x_i}{\partial x_k}\right)\\&-\bar{\sigma}_{PN}^{1-p_n}\left(\sum_{i=1}^n \bar{\sigma}_i^{p_n-2}x_i^q\boldsymbol{\sigma}_i^T\mathbf{T}\mathbf{E}_0\mathbf{B}_i\mathbf{L}_i\mathbf{K}^{-1}\frac{\partial \mathbf{K}}{\partial x_k}\mathbf{u}\right)\end{aligned} \tag{19}$$

Introduction of virtual displacement vectors **u*** using the adjoint method so that Eq (20) holds.

$$\mathbf{K}\mathbf{u}^* = \sum_{i=1}^n \bar{\sigma}_i^{p_n-2}x_i^q\left(\mathbf{E}_0\mathbf{B}_i\mathbf{L}_i\right)^T\mathbf{T}\boldsymbol{\sigma}_i \tag{20}$$

Finally, by substituting Eq (15) into Eq (20), the stress sensitivity is finally obtained as follows:

$$\frac{\partial \bar{\sigma}_{PN}}{\partial x_k} = \frac{q}{x_k}\bar{\sigma}_{PN}^{1-p_n}\bar{\sigma}_k^{p_n} - \bar{\sigma}_{PN}^{1-p_n}\mathbf{u}^{*T}\frac{\partial \mathbf{K}}{\partial x_k}\mathbf{u} \tag{21}$$

From the above equations, the sensitivity analysis is based on the solution of the derivatives of the stiffness matrix and the mass matrix with respect to the variable x. The expressions are as follows:

$$\begin{cases}\dfrac{\partial \mathbf{K}}{\partial x_i} = \dfrac{\partial}{\partial x_i}\left(\sum_{i=1}^n \int \mathbf{B}_i^{\mathrm{T}}\mathbf{E}_i(x_i)\mathbf{B}_i \mathrm{d}v_i\right) = p\sum_{i=1}^n \int \mathbf{B}_i^{\mathrm{T}}x_i^{p-1}(\mathbf{E}-\mathbf{E}_0)\mathbf{B}_i \mathrm{d}v_i\\ \dfrac{\partial \mathbf{M}}{\partial x_i} = \dfrac{\partial}{\partial x_i}\left(\sum_{i=1}^n \int \rho_i\,\mathbf{N}^T\mathbf{N}dv_i\right) = \sum_{i=1}^n \int \rho_0\,\mathbf{N}^T\mathbf{N}dv_i\end{cases} \tag{22}$$

3.1.4. Topology results and post-processing

The topology optimizations of the connecting brackets for the three-axle cargo truck converged after 94, 120 and 45 iterations, respectively. The iterative curves for the objective function of the connecting brackets during the optimization are given in Figure 7, demonstrating the optimized changes in the volume fraction of the materials. In the iterative process, the volume fraction of the three connecting brackets first decreased sharply under the condition that the optimization constraints are guaranteed to be effective; it then fluctuated slightly during the iterative process before finally reaching a steady state. Compared with the topological space, the total volume changed dramatically, and there is a clear trend of material distribution under extreme load conditions. After optimization, the stiffness, strength, and first-order constrained mode of the brackets were improved.

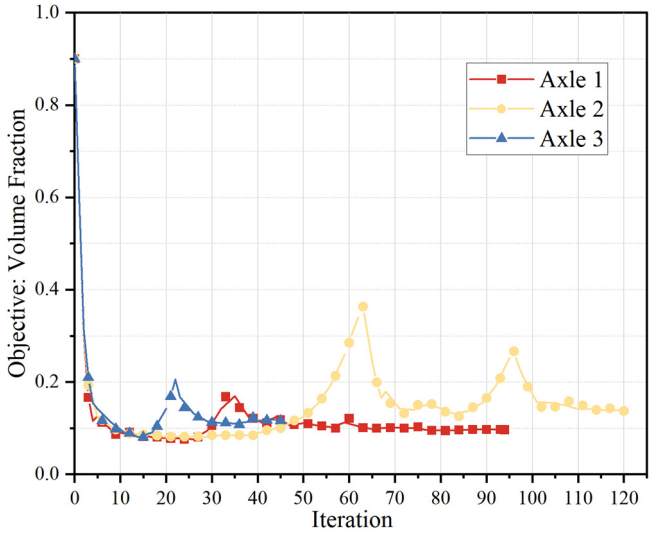

Figure 7. Iterative curves for the objective function.

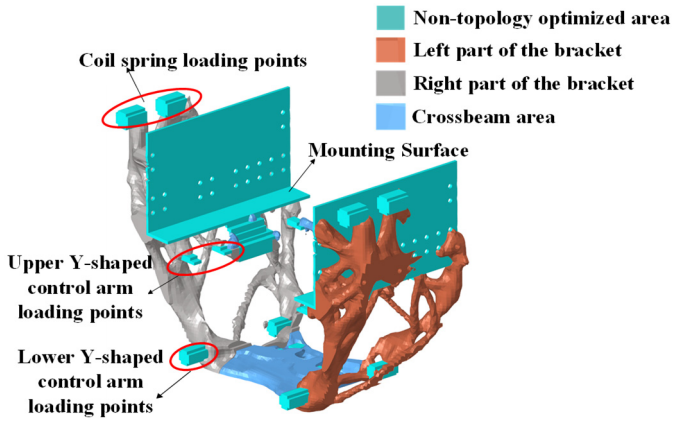

(a) Isometric view of bracket in 1st axle

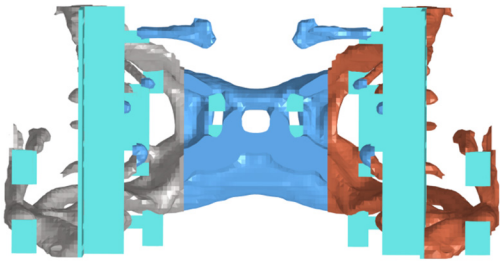

(b) Planform view of bracket in 1st axle

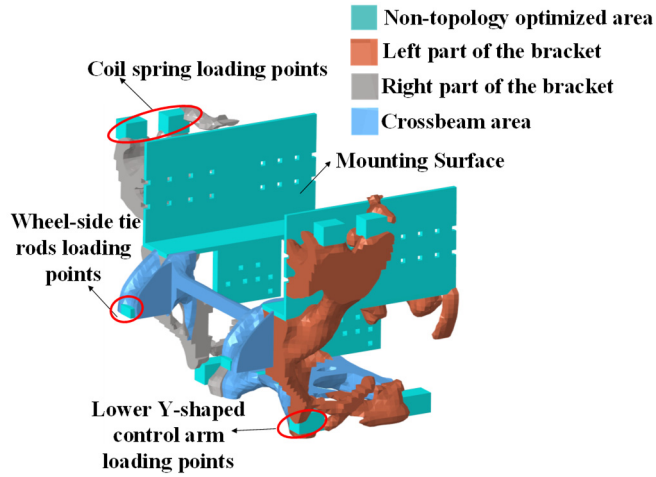

(c) Isometric view of bracket in 2nd axle

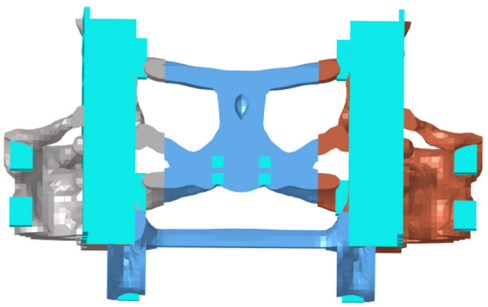

(d) Planform view of bracket in 2nd axle

Continued on next page

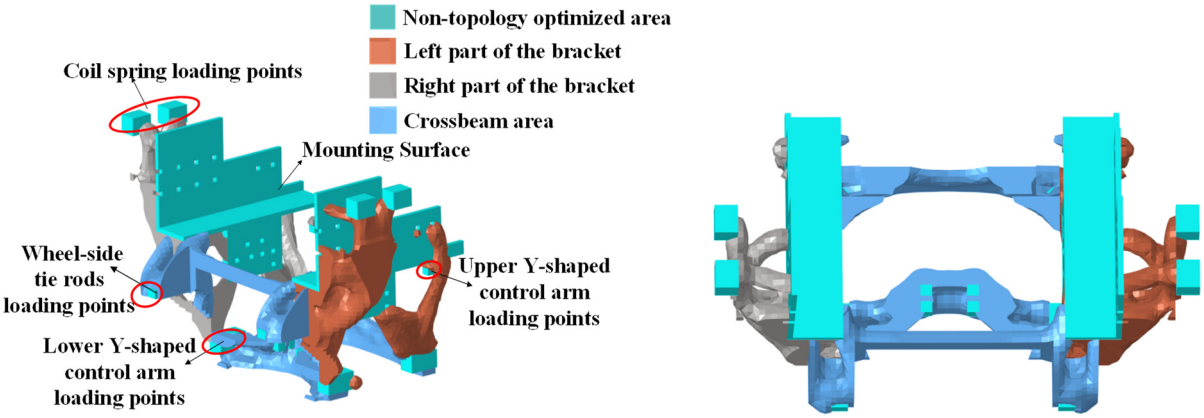

(e) Isometric view of bracket in 3rd axle (f) Planform view of bracket in 3rd axle

Figure 8. Topology optimization results for three-axle cargo truck bracket.

The topology optimization results are shown in Figure 8. The deformation, stress and mode clouds of the optimized topology results are given in Appendix.

However, the optimization results are often not directly manufacturable. As a conceptual model, the topology optimization results are used as a reference to create new connecting brackets. The topology results shown in Figure 8 were converted into a geometric model and imported into the integrated CAD/CAE/CAM software for the next processing step. The non-topology areas are the mounting surface and the loading point, respectively. As shown in Figure 9, the plates of the mounting surface in contact with the frame were modified in shape according to the connecting bolts' layout. The connecting surface with the gearbox housing was designed according to the housing size and the bolt positions. The positions of the loading point had been determined, from which the positions of the plates were obtained rigidly connected to it. The material at these locations was eliminated to avoid interference between the bracket and the coil spring, and to leave room for moving the Y-shaped upper and lower control arms and the wheel half-axle. Taking Figure 8(a) as an example, the material was expanded at the locations of the coil spring loading points in the topology area. The material extended from the coil spring to the lower control arm to form a force transmission path so that multiple ear-shaped side plates could be designed; thus, the bracket body plate was designed. Then, transverse and longitudinal reinforcement plates were set according to the locations where the material remained in the topology result. Considering the manufacturing difficulties, the reinforcement plates were also appropriately adjusted during the design process. Figure 8(b) gives the general shape of the bottom design space, from which the rectangular plate member was designed. We added reinforcement plates to the plate, and the material was subtracted appropriately according to the topology result of material thickness. The new connecting bracket is a combined structure welded by multiple steel plates, and the connecting bracket mainly uses shell elements to divide the mesh. The bolted connections between the components were simulated by solid elements. The boundary condition of the improved model was set to six degrees of freedom at the connecting bracket and frame bolt connection, as shown in Figure 9.

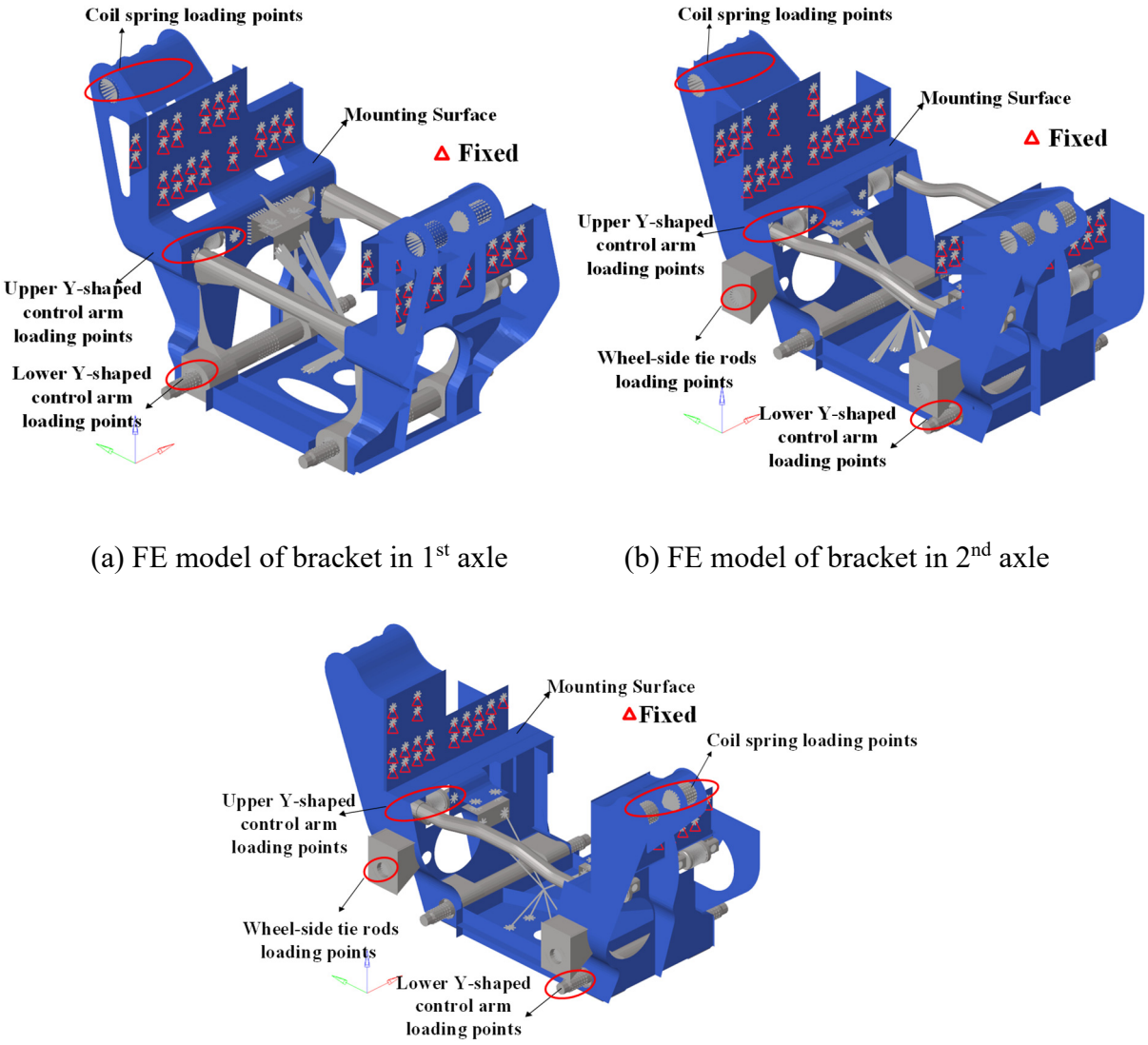

(a) FE model of bracket in 1st axle

(b) FE model of bracket in 2nd axle

(c) FE model of bracket in 3rd axle

Figure 9. Finite element (FE) models for size optimization.

3.2. Size optimization process

In the subsequent detailed design, the size optimization method is used to make the structure of the modified connecting bracket sheet metal parts more reasonable. The size optimization finite element model increases the design space of the lower end of the brackets to connect the brackets to the lower Y-shaped control arm. In addition, considering the mounting load on the main gearbox housing, the bottom design space was increased. As shown in Figure 10, the three connecting brackets consisted of 22, 17 and 16 plate members, whose thicknesses were employed as design variables for size optimization. Each plate member was designed to have a corresponding thickness interval. The initial thickness variables of all plates were set to 12 mm.

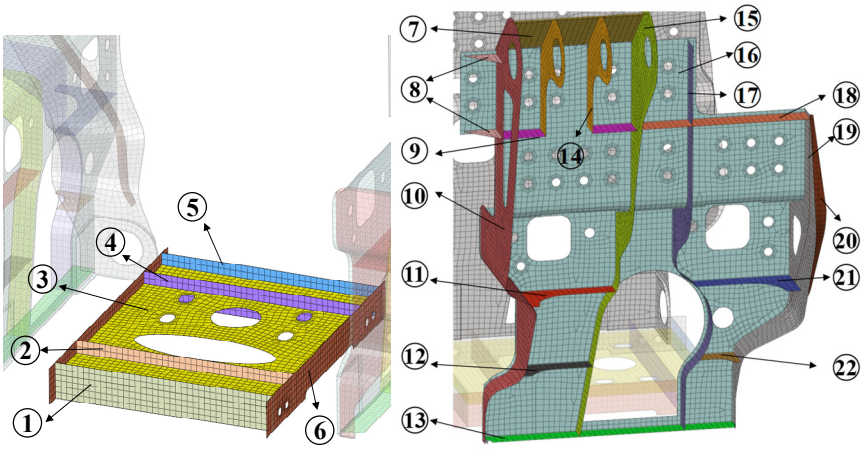

(a) Design variables of bracket in 1st axle

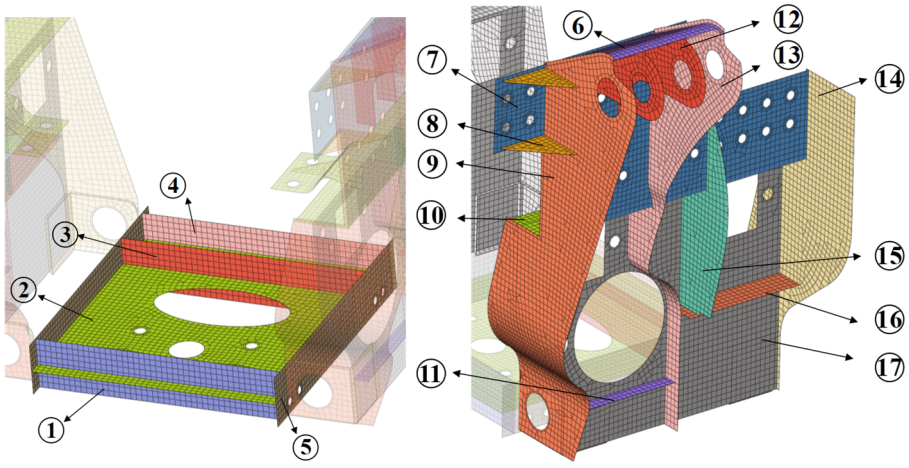

(b) Design variables of bracket in 2nd axle

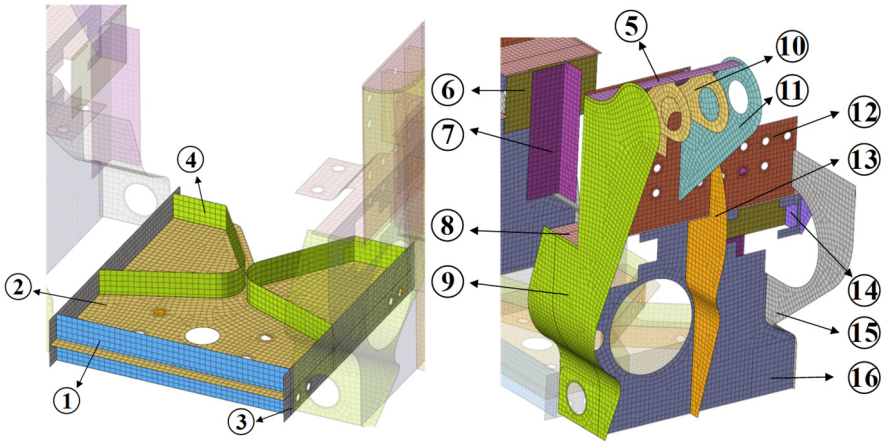

(c) Design variables of bracket in 3rd axle

Figure 10. Design variables for size optimization.

Along with considering the influence of the static load of each working condition on the connecting bracket, the power spectral density (PSD) curve for the random vibration signal generated during the endurance road test was applied as the load spectrum for the connecting bracket. The root-mean-square (RMS) stress of the bracket was constrained to further ensure the structure's durability and prevent fatigue damage [40]. Off-roading was taken as the working condition extracted for autocorrelation; then, a Fourier transform was carried out according to the Wiener-Sinchin theorem to obtain the PSD loading curve, as shown in Figure 11.

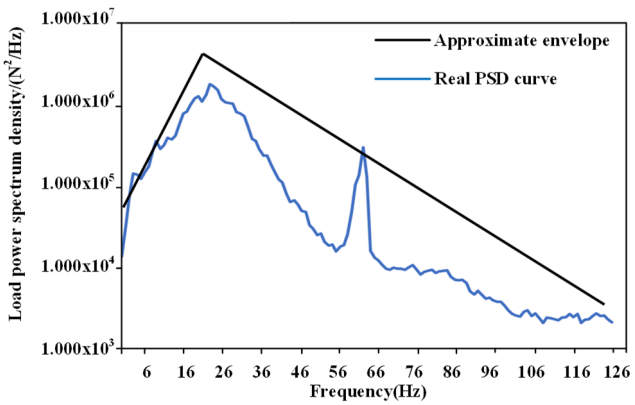

(a) Loading curve in 1st axle

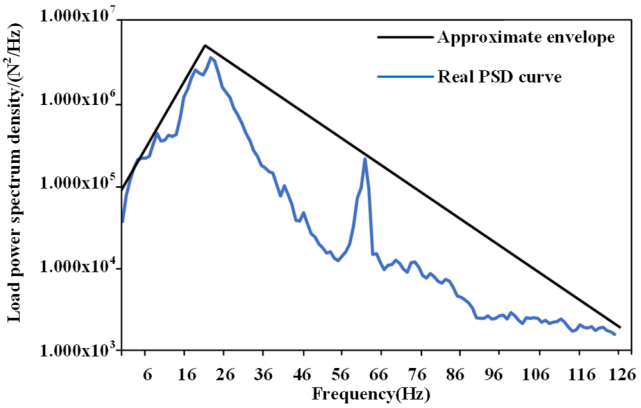

(b) Loading curve in 2nd axle

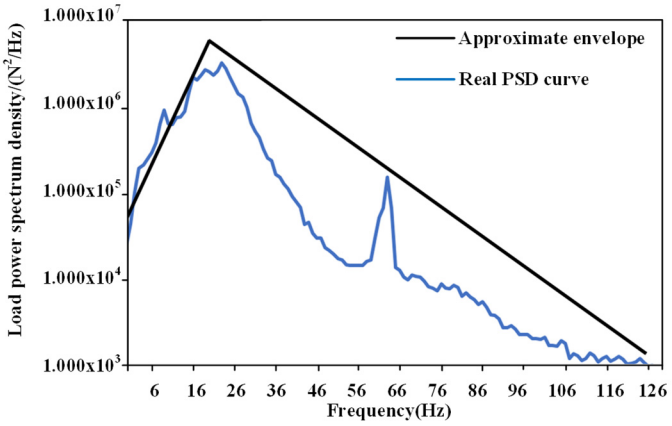

(c) Loading curve in 3rd axle

Figure 11. Examples of PSD loading curves for the hard point of the left coil spring.

Based on the previous performance constraint, the size optimization limits the RMS stress of the bracket to no more than 100 MPa. The size optimization problem for the improved structure of the connecting brackets can be formulated as follows:

$$\begin{cases} \text{find: } \mathbf{x} = [x_1, x_2, x_3, \ldots, x_{17}]^T \\ \text{Minimize: } V(x) \\ Subject\ to: \sigma_{vm,i}^l \le \tilde{\sigma}_0, i = 1,2,\ldots 17; l = 1,2,3 \ldots 5 \\ \qquad \sigma_{RMS,i} \le \tilde{\sigma}_0, i = 1,2,\ldots 17 \\ \qquad d_j^l \le \tilde{d}^l, j = 1,2,3,\ldots 12 \\ \qquad \omega_k \ge \tilde{\omega}_0 \\ \qquad x_i \in int([6,20]) \end{cases} \tag{23}$$

The iterative curves for the objective function are illustrated in Figure 12. Compared with the total mass of the original connecting bracket, the mass of the optimal connecting bracket was reduced by 15.2%, as listed in Table 3, while the performance of the bracket was improved. The critical parameters of the optimal connecting bracket are listed in Table 4.

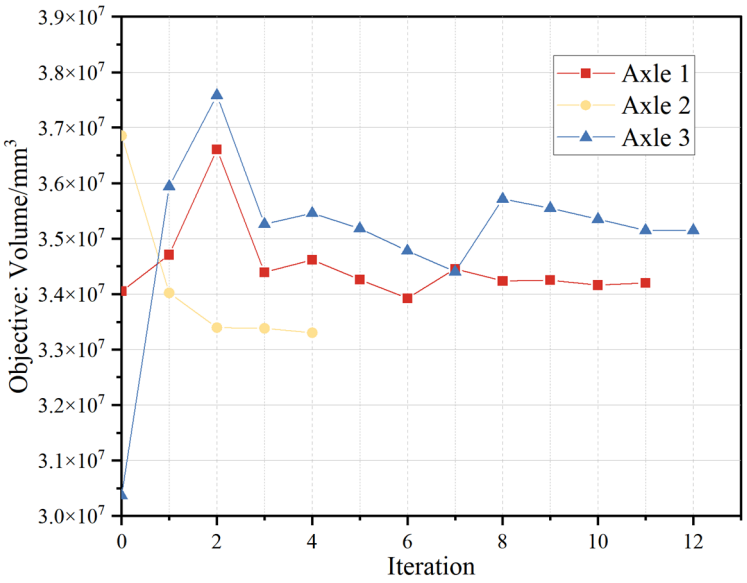

Figure 12. Iterative curves for the objective function.

Table 3. Comparison of bracket optimization results (10^7 mm^3).

Axle	Volume of original bracket	Volume of optimized bracket
1	4.254	3.431
2	4.2	3.337
3	3.675	3.514

Table 4. Size optimization results (mm).

Axles	Variable index	Min	Max	Optimization result
1	$x_{1\sim3}$, $x_{11\sim13}$	6	20	8
	x_4	6	20	14
	$x_{5\sim6}$	6	20	18

Continued on next page

Axles	Variable index	Min	Max	Optimization result
1	$x_{7\sim9}$, $x_{17\sim18}$, $x_{20\sim21}$	6	20	6
	x_{10}, x_{16}	6	15	15
	$x_{14\sim15}$	6	20	12
	x_{19}	6	15	9
	x_{22}	6	20	10
2	x_1, x_{10}, x_{12}	6	20	8
	x_2	6	20	13
	$x_{3\sim4}$, x_6, x_8, x_{11}, $x_{14\sim16}$	6	20	6
	x_5, x_7	6	20	11
	x_9, x_{13}	6	15	15
	x_{13}	6	15	6
3	x_1	6	20	16
	x_2, x_{16}	6	20	12
	x_3, x_{14}	6	20	10
	x_4, $x_{6\sim8}$	6	20	7
	x_5	6	20	15
	x_9, x_{15}	6	15	15
	$x_{10\sim12}$	6	20	20
	x_{13}	6	15	8

4. Validation of optimal design

A fatigue life analysis of the structure was performed, and endurance road tests were applied to a three-axle cargo vehicle equipped with the new connecting bracket, verifying the safety of the optimal connection bracket. After applying the off-road load spectrum, the fatigue damage under the effect of a single-cycle load spectrum was derived as shown in Figure 13. Based on Eq (1), the fatigue damage values for a 6000-km distance were calculated; the results are shown in Table 5. Compared with the fatigue damage results for the original bracket, the maximum single damage for off-road excitation was reduced by about 10^{-10} times. The converted damage values for the three bridges under off-road conditions were all less than 1. This indicates no potential fatigue damage risk for the bridge box attachment bracket under fatigue loading.

The brackets were also verified through manufacturing and testing, and the fatigue results obtained from the endurance road test were compared with the original brackets' fatigue test results. As shown in Figure 14, the optimal bracket installed in the three-axle cargo truck was in excellent condition without fatigue damage. This result meets the safety requirements.

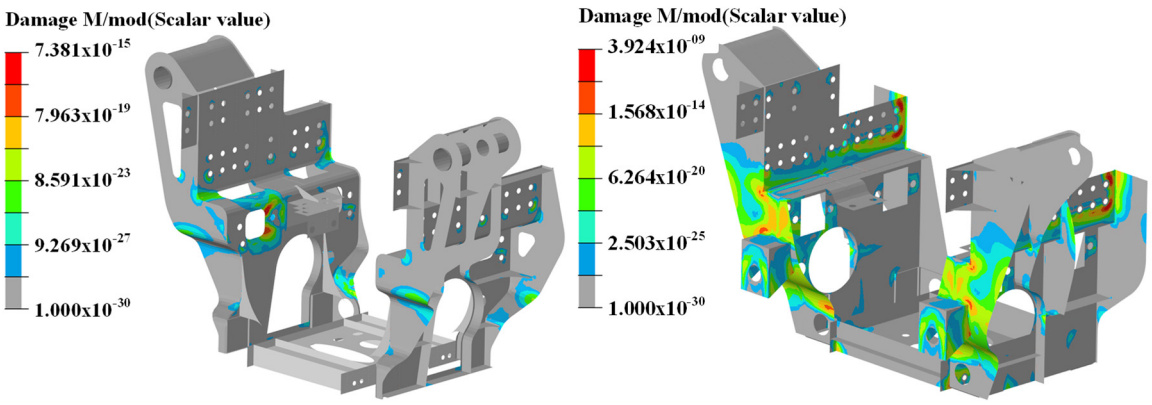

(a) Bracket in 1st axle (b) Bracket in 2nd axle

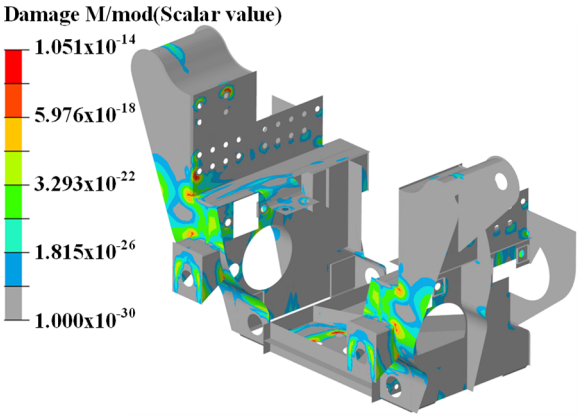

(c) Bracket in 3rd axle

Figure 13. Fatigue damage under the effect of a single cycle load spectrum.

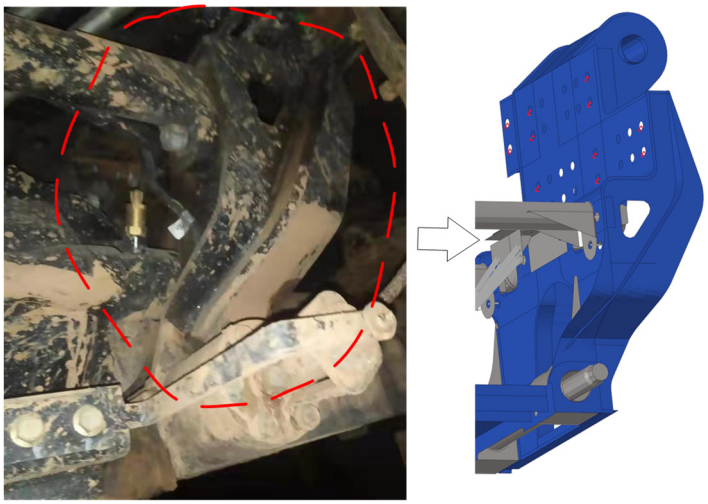

(a) Bracket in 1st axle

Continued on next page

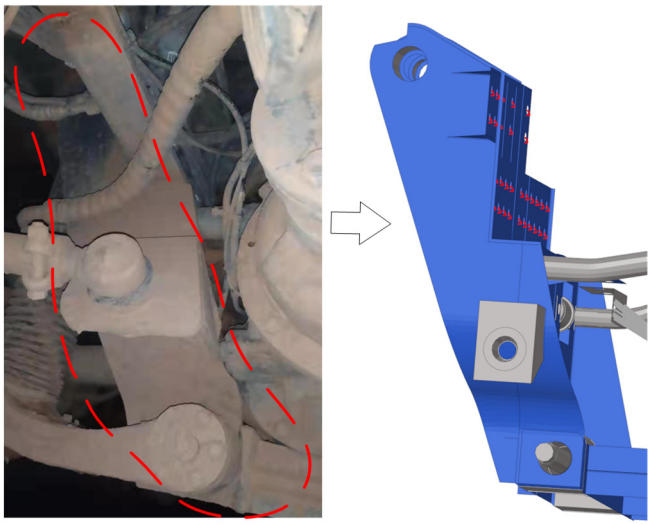

(b) Bracket in 2nd axle

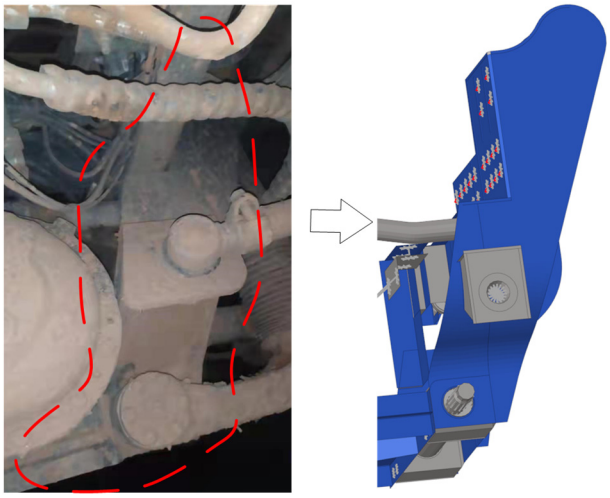

(c) Bracket in 3rd axle

Figure 14. Prototypes of connecting bracket after testing.

Table 5. Comparison of cumulative damage values D.

Axle	Cumulative damage value (D) of the original bracket	Cumulative damage values (D) of the optimized bracket
1	1.938	1.197×10^{-11}
2	2.822	6.363×10^{-6}
3	7.049×10^{-3}	1.704×10^{-11}

5. Conclusions

1) In this paper, a complete optimization design verification process has been proposed to provide

practical ideas and utility value for developing multi-performance suspensions in the pre-product development phase. First, a vehicle endurance road test was applied to a three-axle cargo truck with its original connection brackets; the corresponding finite element analysis was conducted to verify the results. Topology optimization and size optimization have been proposed as two necessary optimization steps. In the topology optimization process, multiple constraint performance measures, such as the displacement at the loading point for each working condition, global von Mises stress and first-order constrained mode, are considered. A novel layout of the connecting bracket was obtained by using the SIMP method. A size optimization method has been presented to optimize the connecting bracket further and obtain the optimal plate thickness. An optimal structure with a 15.2% weight reduction was obtained while maintaining better stiffness and durability. Finally, the optimal design for the fatigue analysis and road tests was implemented. The experimental results were in good agreement with the simulation results.

2) A novel structure of the connecting brackets has been proposed to solve the problem of fatigue failure of the original bracket. The connecting bracket is one of the essential connecting parts of the cargo truck, and it bears the tremendous and complex load of road excitation during the working process. The optimized connecting brackets have higher strength, higher stiffness and better durability. At the same time, the structure meets the weight limits of relevant standards, reducing material consumption.

6. Data availability

The data that support the findings of this study are available from Beiben Trucks Group Co., Ltd., but restrictions apply regarding the availability of these data, which were used under license for the current study and are thus not publicly available.

Acknowledgments

This work was supported by the National Key Research and Development Program of China (grant number 2016YFB0101602), the National Natural Science Foundation of China (grant number 51575399) and the Project of Shanghai Science and Technology Committee (grant number 20511104601). FX and YG appreciate the financial support from these grants.

Conflict of interest

The authors have no relevant financial or non-financial interests to disclose.

References

1. A. C. R. Teixeira, P. G. Machado, F. M. de Almeida Collaço, D. Mouette, Alternative fuel technologies emissions for road heavy-duty trucks: a review, *Environ. Sci. Pollut. Res.*, **28** (2021), 20954−20969. https://doi.org/10.1007/s11356-021-13219-8
2. T. Kuczek, Application of manufacturing constraints to structural optimization of thin-walled structures, *Eng. Optim.*, **48** (2016), 351−360. https://doi.org/10.1080/0305215X.2015.1017350

3. K. T. Cheng, N. Olhoff, An investigation concerning optimal design of solid elastic plates, *Int. J. Solids Struct.*, **17** (1981), 305−323. https://doi.org/10.1016/0020-7683(81)90065-2
4. M. P. Bendsoe, N. Kikuchi, Generating optimal topologies in structural design using a homogenization method, *Comput. Methods Appl. Mech. Eng.*, **71** (1988), 197−224. https://doi.org/10.1016/0045-7825(88)90086-2
5. M. P. Bendsoe, O. Sigmund, Material interpolation schemes in topology optimization, *Arch. Appl. Mech.*, **69** (1999), 635−654. https://doi.org/10.1007/s004190050248
6. J. M. Martínez, A note on the theoretical convergence properties of the SIMP method, *Struct. Multidiscip. Optim.*, **29** (2005), 319−323. https://doi.org/10.1007/s00158-004-0479-8
7. M. Stolpe, K. Svanberg, An alternative interpolation scheme for minimum compliance topology optimization, *Struct. Multidiscip. Optim.*, **22** (2001), 116−124. https://doi.org/10.1007/s001580100129
8. H. Zhang, X. H. Ren, Topology optimization of continuum structures based on SIMP, *Adv. Mater. Res.*, Trans Tech Publications, Ltd., **255–260** (2011), 14–19. https://doi.org/10.4028/www.scientific.net/AMR.255-260.14
9. W. J. Zuo, J. T. Bai, J. F. Yu, Sensitivity reanalysis of static displacement using Taylor series expansion and combined approximate method, *Struct. Multidiscip. Optim.*, **53** (2016), 953−959. https://doi.org/10.1007/s00158-015-1368-z
10. K. T. Zuo, L. P. Chen, Y. Q. Zhang, J. Yang, Manufacturing- and machining-based topology optimization, *Int. J. Adv. Manuf. Technol.*, **27** (2006), 531−536. https://doi.org/10.1007/s00170-004-2210-8
11. X. J. Gao, L. J. Li, H. T. Ma, An adaptive continuation method for topology optimization of continuum structures considering buckling constraints, *Int. J. Appl. Mech.*, **9** (2017). https://doi.org/10.1142/S1758825117500922
12. S. Z. Xu, J. K. Liu, B. Zou, Q. H. Li, Y. S. Ma, Stress constrained multi-material topology optimization with the ordered SIMP method, *Comput. Methods Appl. Mech. Eng.*, **373** (2021). https://doi.org/10.1016/j.cma.2020.113453
13. Y. F. Bai, M. Cong, Y. Y. Li, Structural topology optimization for a robot upper arm based on SIMP method, in *3rd IEEE/IFToMM/ASME International Conference on Reconfigurable Mechanisms and Robots (ReMAR)*, 2015. https://doi.org/10.1007/978-3-319-23327-7_62
14. B. Mohamodhosen, F. Gillon, A. Tounzi, L. Chevallier, J. Korecki, Topology optimisation of a 3D electromagnetic device using the SIMP density-based method, in *2016 IEEE Conference on Electromagnetic Field Computation (CEFC)*, IEEE, Miami, FL, 2016. https://doi.org/10.1109/CEFC.2016.7816001
15. G. L. Srinivas, S. P. Singh, A. Javed, Experimental evaluation of topologically optimized manipulator-link using PLC and HMI based control system, in *3rd International E-Conference on Frontiers in Mechanical Engineering and NanoTechnology (ICFMET)*, 2020. https://doi.org/10.1016/j.matpr.2020.08.023
16. Q. Liu, X. K. Ma, Y. Z. Lin, Z. J. Zong, Topology and sizing optimization of light-weight frame for energy-saving vehicle, in *International Conference on Advanced Design and Manufacturing Engineering (ADME 2011)*, Trans Tech Publications Ltd., 2011. https://doi.org/10.4028/www.scientific.net/AMR.308-310.1220

17. B. Torstenfelt, A. Klarbring, Conceptual optimal design of modular car product families using simultaneous size, shape and topology optimization, *Finite Elem. Anal. Des.*, **43** (2007), 1050−1061. https://doi.org/10.1016/j.finel.2007.06.005
18. L. Wang, X. K. Chen, Q. H. Zhao, Muti-objective topology optimization of an electric vehicle's traction battery enclosure, in *Applied Energy Symposium and Summit - Low Carbon Cities and Urban Energy Systems (CUE)*, 2015. https://doi.org/10.1016/j.egypro.2016.06.103
19. J. G. Cho, J. S. Koo, H. S. Jung, A lightweight design approach for an EMU carbody using a material selection method and size optimization, *J. Mech. Sci. Technol.*, **30** (2016), 673−681. https://doi.org/10.1007/s12206-016-0123-8
20. S. B. Lu, H. G. Ma, W. J. Zuo, Lightweight design of bus frames from multi-material topology optimization to cross-sectional size optimization, *Eng. Optim.*, **51** (2019), 961−977. https://doi.org/10.1080/0305215X.2018.1506770
21. J. Bai, Y. Zhao, G. Meng, W. Zuo, Bridging topological results and thin-walled frame structures considering manufacturability, *J. Mech. Des.*, **143** (2021). https://doi.org/10.1115/1.4050300
22. H. Ma, J. Wang, Y. Lu, Y. Guo, Lightweight design of turnover frame of bridge detection vehicle using topology and thickness optimization, *Struct. Multidiscip. Optim.*, **59** (2019), 1007−1019. https://doi.org/10.1007/s00158-018-2113-1
23. G. Y. Sun, D. D. Tan, X. J. Lv, X. L. Yan, Q. Li, X. D. Huang, Multi-objective topology optimization of a vehicle door using multiple material tailor-welded blank (TWB) technology, *Adv. Eng. Software*, **124** (2018), 1−9. https://doi.org/10.1016/j.advengsoft.2018.06.014
24. J. Zhang, L. Ning, Y. Hao, T. Sang, Topology optimization for crashworthiness and structural design of a battery electric vehicle, *Int. J. Crashworthiness*, **26** (2021), 651−660. https://doi.org/10.1080/13588265.2020.1766644
25. D. J. Munk, J. D. Miller, Topology optimization of aircraft components for increased sustainability, *AIAAJ*, **60** (2022), 445−460. https://doi.org/10.2514/1.J060259
26. Y. L. Lee, M. E. Barkey, H. T. Kang, *Metal Fatigue Analysis Handbook: Practical Problem-Solving Techniques for Computer-Aided Engineering*, Burlington: Elsevier Butterworth-Heinemann, (2012), 1−580. https://doi.org/10.1016/C2010-0-66376-0
27. C. H. Wang, M. W. Brown, Life prediction techniques for variable amplitude multiaxial fatigue−Part 2: comparison with experimental results, *J. Eng. Mater. Technol.*, **118** (1996), 371−374. https://doi.org/10.1115/1.2806822
28. S. H. Jeong, J. W. Lee, G. H. Yoon, D. H. Choi, Topology optimization considering the fatigue constraint of variable amplitude load based on the equivalent static load approach, *Appl. Math. Model.*, **56** (2018), 626−647. https://doi.org/10.1016/j.apm.2017.12.017
29. R. T. Haftka, Z. Gürdal, M. P. Kamat, Elements of structural optimization, Kluwer Academic Publishers, 1991. https://doi.org/10.1007/978-94-015-7862-2
30. D. L. Shu, *Mechanical Property of Engineering Material*, Beijing, China: China Machine Press, 2007. Available from: https://ss.zhizhen.com/detail_38502727e7500f26a296ae892b789bcc44b4f281d9485a991921b0a3ea25510134114c969f2eae5c13747adaf1f08d1c325955064941cd542e24c1535a7f8b4287df4e09375dba6c27789fd2eaaf69be.
31. A. Li, C. S. Liu, Lightweight design of a crane frame under stress and stiffness constraints using super-element technique, *Adv. Mech. Eng.*, **9** (2017), 15. https://doi.org/10.1177/1687814017716621

32. O. Sigmund, J. Petersson, Numerical instabilities in topology optimization: a survey on procedures dealing with checkerboards, mesh-dependencies and local minima, *Struct. Optim.*, **16** (1998), 68−75. https://doi.org/10.1007/BF01214002
33. K. Svanberg, The method of moving asymptotes—a new method for structural optimization, *Int. J. Numer. Methods Eng.*, **24** (1987), 359−373. https://doi.org/10.1002/nme.1620240207
34. Z. Hu, S. Sun, O. Vambol, K. Tan, Topology optimization of laminated composite structures under harmonic force excitations, *J. Compos. Mater.*, **56** (2022), 409−420. https://doi.org/10.1177/00219983211052605
35. Q. Q. Liang, Y. M. Xie, G. P. Steven, Optimal topology selection of continuum structures with displacement constraints, *Comput. Struct.*, **77** (2000), 635−644. https://doi.org/10.1016/S0045-7949(00)00018-3
36. X. J. Yang, J. Zheng, S. Y. Long, Topology optimization of continuum structures with displacement constraints based on meshless method, *Int. J. Mech. Mater. Des.*, **13** (2017), 311−320. https://doi.org/10.1007/s10999-016-9337-2
37. M. Bruggi, On an alternative approach to stress constraints relaxation in topology optimization, *Struct. Multidiscip. Optim.*, **36** (2008), 125−141. https://doi.org/10.1007/s00158-007-0203-6
38. C. Le, J. Norato, T. Bruns, C. Ha, D. Tortorelli, Stress-based topology optimization for continua, *Struct. Multidiscip. Optim.*, **41** (2010), 605−620. https://doi.org/10.1007/s00158-009-0440-y
39. S. H. Jeong, S. H. Park, D. H. Choi, G. H. Yoon, Topology optimization considering static failure theories for ductile and brittle materials, *Comput. Struct.*, **110** (2012), 116−132. https://doi.org/10.1016/j.compstruc.2012.07.007
40. X. J. Peng, Fatigue Estimation based on Stress RMS under Stochastic Excitation, in *2nd International Conference on Advanced Electronic Materials, Computers and Materials Engineering (AEMCME)*, 2019. https://doi.org/10.1088/1757-899X/563/4/042058

Appendix

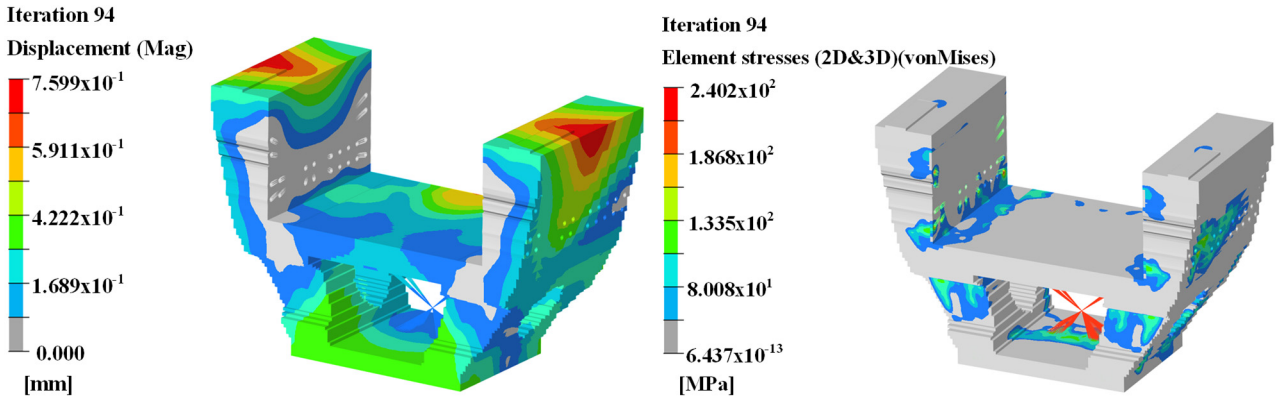

(a) Displacement (b) Elemental stress

Continued on next page

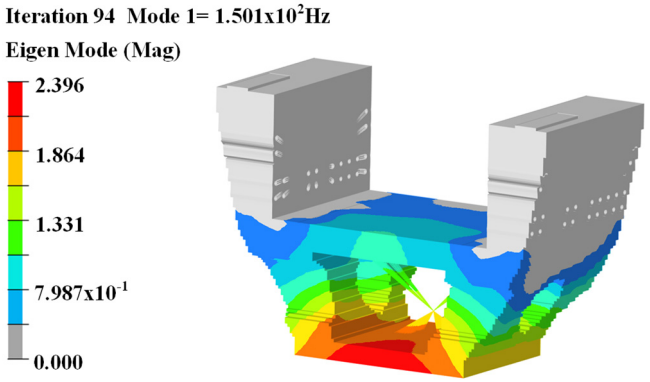

(c) Constraint mode

Figure A1. FE analysis of topology optimization results for the first axle.

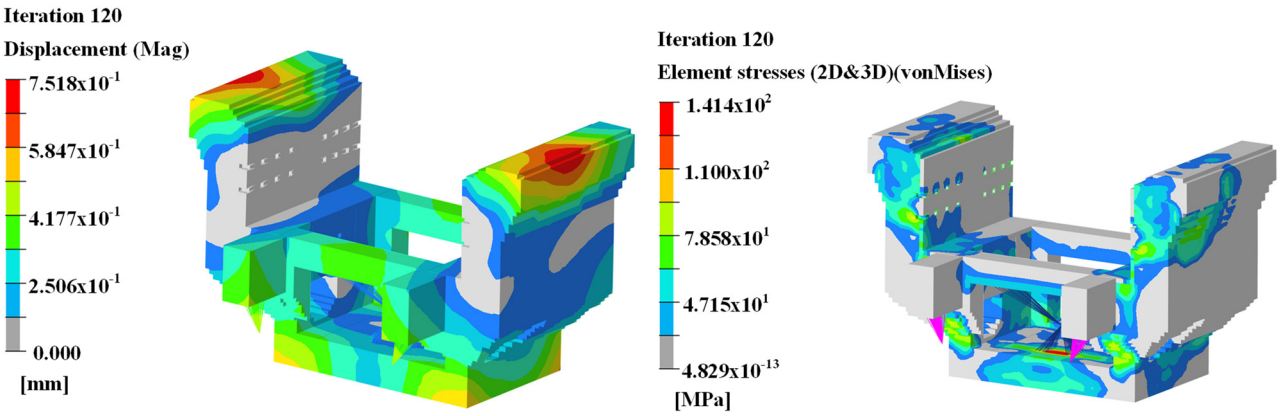

(a) Displacement

(b) Elemental stress

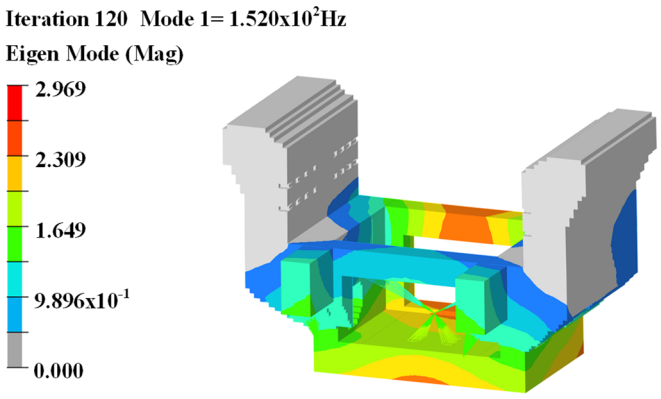

(c) Constraint mode

Figure A2. FE analysis of topology optimization results for the second axle.

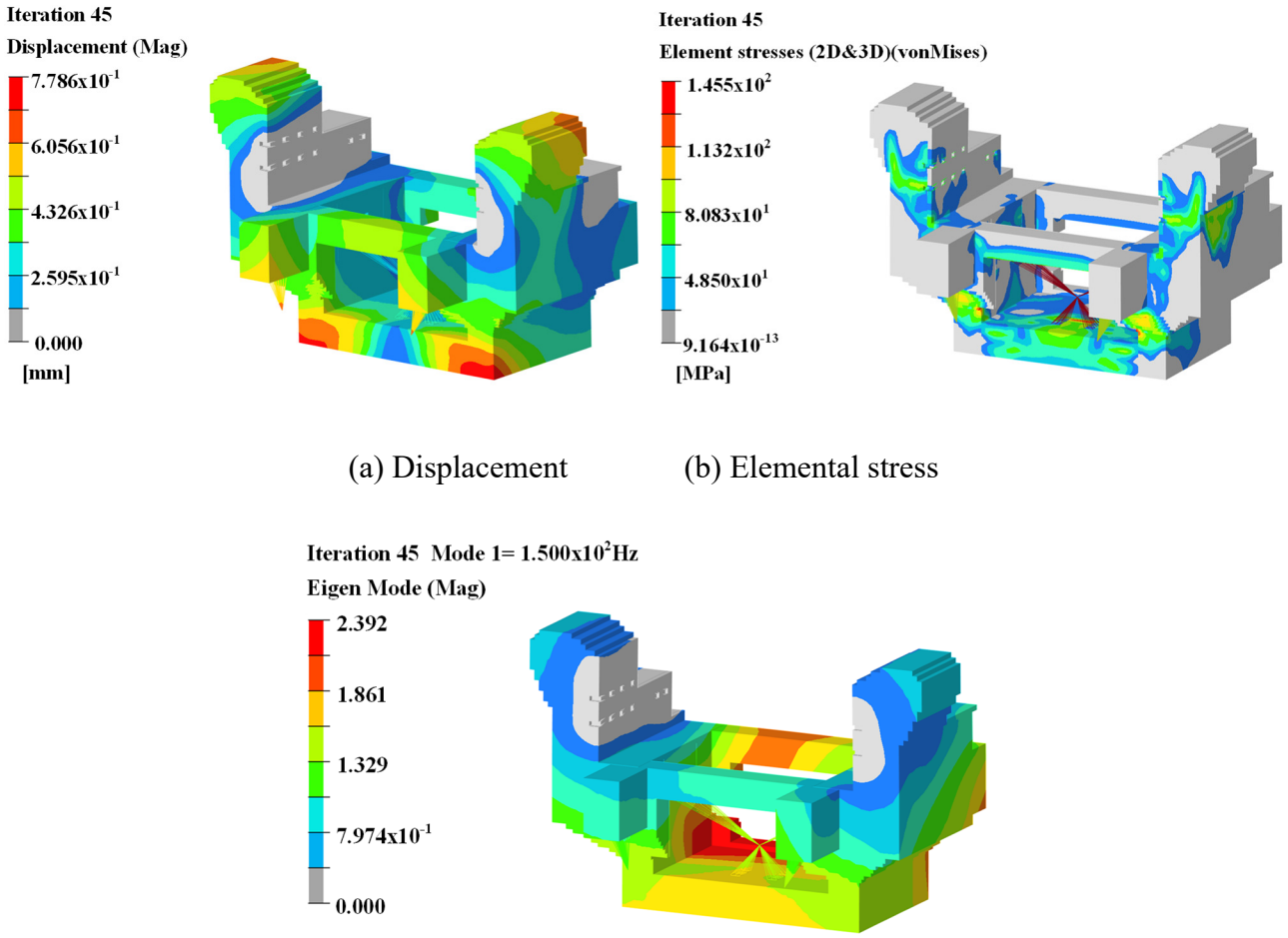

(a) Displacement (b) Elemental stress

(c) Constraint mode

Figure A3. FE analysis of topology optimization results for the third axle.